A DIRECT TRACKING METHOD FOR A GROUNDED CONDUCTOR INSIDE A PIPELINE FROM CAPACITANCE MEASUREMENTS

By

Hyenkyun Woo

Sungwhan Kim

Jin Keun Seo

William Lionheart

and

Eung Je Woo

IMA Preprint Series # 2097

(February 2006)

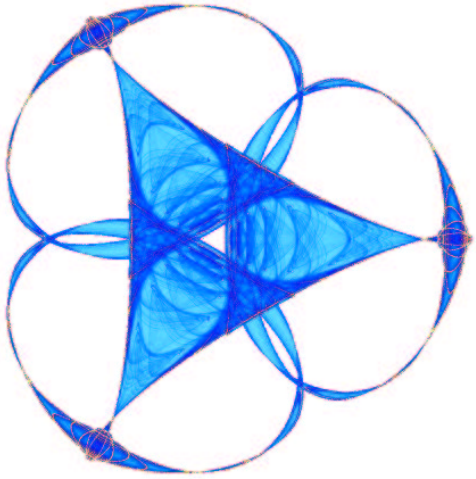

INSTITUTE FOR MATHEMATICS AND ITS APPLICATIONS

UNIVERSITY OF MINNESOTA

400 Lind Hall

207 Church Street S.E.

Minneapolis, Minnesota 55455–0436

Phone: 612/624-6066 Fax: 612/626-7370

URL: http://www.ima.umn.edu

A direct tracking method for a grounded conductor inside a pipeline from capacitance measurements

Hyenkyun Woo†, Sungwhan Kim‡, Jin Keun Seo†, William Lionheart§ and Eung Je Woo♯

† Department of Mathematics, Yonsei University, Korea
‡ Graduate School of Mathematical Sciences, the University of Tokyo, Japan
§ School of Mathematics, University of Manchester, UK
♯ College of Electronics and Information, Kyung Hee University, Korea

Abstract. We present a new non-iterative method for tracking conductive water in a pipeline using a single excitation pattern from an interleaved ECT system. The problem arises for example in the oil industry where brine is often mixed with oil in a pipeline. If the size of the body of brine is very large compared with the size of electrodes attached to the pipeline, the corresponding electric potential in the region of brine is close to zero. This model leads to the inverse problem of identifying the dynamic change of the cross-section of a grounded conducting region in a pipeline. Unfortunately, standard iterative reconstruction algorithms in ECT associated with the sensitivity matrix do not work in this case. Furthermore, due to unavailability of the Neumann data at drive electrodes, the previously published layer potential methods for capturing the inhomogeneity are not applicable to this system. In this work, we derive a formula providing a concrete relation between the capacitance change in each receive electrode and the dynamical change in a grounded conducting region inside the pipeline. The proposed method successfully reconstructs feature information such as location and rough shape of the cross section of the water region. We demonstrate the performance of our method in numerical simulations and actual experiments.

1. Introduction

Electrical capacitance tomography (ECT) is a real-time imaging technology that has been developed for visualizing dynamical changes of the permittivity distribution in the form of cross-sectional image in pipeline. In ECT, electrical capacitance sensors are attached symmetrically around the periphery of an insulating pipe to measure the capacitance change due to the change in internal permittivity of the material. We apply a positive voltage to selected electrodes while grounding the other electrodes in order to generate an electric field inside the pipe. We then measure the inter-electrode capacitances. With N electrodes, there are $N(N-1)/2$ independent capacitance measurements that can be obtained by driving each electrode in sequence. In a standard ECT system (Yang 1996; Yang and York 1999), these $N(N-1)/2$ independent measurements are used to estimate a cross-sectional permittivity image in pipeline.

In this work, we consider an ECT system for visualizing the flow of a mixture of oil and water in a pipeline. This problem arises in the oil extraction industry where water is injected in an reservoir to force out the oil. Both water and oil appear in the pipeline and estimating the fraction of water is an important issue. The water typically has a high salt content and is therefore highly conductive. In one possible flow regime, the salt water occupies a region inside the pipe and is surrounded by oil which has a much lower permittivity. If the size of water is very large compared with the size of electrodes, the corresponding electric potential in the region of water is close to zero. Our aim is to devise a fast and direct method of reconstructing image of the cross section of water region using the ECT system.

Most of researchers in ECT use standard iterative reconstruction algorithms associated with a sensitivity matrix. Unfortunately, such methods can not be applied to our situation where we try to visualize a grounded conductor region in the pipe. Hence, we need to develop a new ECT reconstruction algorithm to estimate the surface of the grounded conductor, i.e. salt water component.

In this work, we use a single-drive interleaved electrode system. The schematic of our ECT system is depicted in figure 1(a), where 16 receive electrodes and 16 drive electrodes are interleaved. We apply V volt to all drive electrodes while all receive electrodes are grounded. When the permittivity distribution is homogeneous, this produces an electric field with a symmetrical pattern inside the cross-section of the pipeline as shown in figure 1(b). Therefore, the measured standing capacitances are all equal. When a grounded conducting material enters into the pipe, the electric field will be distorted and it gives rise to a decrease of capacitance in each receive electrode. The amount of capacitance decrease measured in each receive electrode can be used to estimate the grounded region.

This kind of ECT system significantly simplifies the hardware complexity and increases its measurement accuracy. When electric switches are used to select electrodes between drive and receive modes, measurement noise occurs from stray capacitances due to the switches. This problem can be eliminated by separating drive and receive

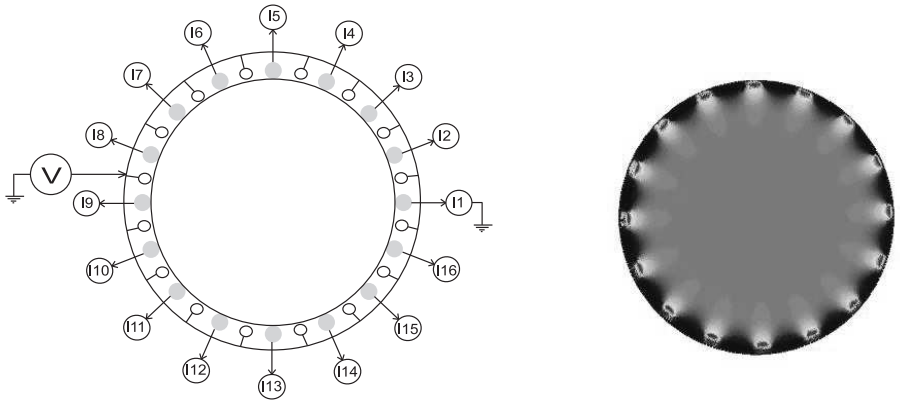

(a) (b)

Figure 1. (a) Sensor configuration of a single-drive interleaved ECT system. (b) Electric potential distribution inside the pipeline of a single-drive interleaved ECT system in the absence of any grounded conducting region.

electrodes. Furthermore, since equally-spaced sixteen drive electrodes are connected to one signal generator, the standing capacitance is the same for all receive electrodes as illustrated in figure 1(b).

In this system, we employ only a single set of measured Neumann data (measured capacitance) because the Dirichlet data (applied voltage) is fixed. Unlike most ECT systems, but in common with some medical electrical imaging systems (Brown *et al* 1994; Zhu *et al* 1994), we do not measure Neumann data on drive electrodes. We pay for this simplification in hardware with mathematical difficulties of incomplete data. In this work, we compensate for the reduced data set by developing a formula providing a concrete relation between capacitance change and the dynamical change of the grounded conducting region inside the pipeline.

At this point, it would be desirable to mention the previously published work (Kim *et al* 2002) that also developed a location search algorithm of a grounded conductor. We initially developed an ECT system for a practical application of this location search formula in Kim *et al* (2002), but unfortunately we could not get a satisfactory result due to the unavailability of Neumann data on drive electrodes. In this model for recovering the grounded conductor, the magnitude of Neumann data at drive electrodes is usually larger than that of the receive electrodes. Furthermore, Neumann data on drive electrodes is very different from that of the surrounding receive electrodes, so its approximation would be difficult and we must consider the ill-posedness of the inverse problem with measurement inaccuracy. This is why we have modified the ECT system and developed a new formula providing a relation between a grounded conductor and capacitance at each receive electrode.

Based on this interleaved ECT system with a single symmetrical excitation pattern, we develop a simple direct method for tracking the dynamical change of a continuous water flow in the pipeline. The proposed method successfully reconstructs feature information such as location and rough shape of the cross section of the water region.

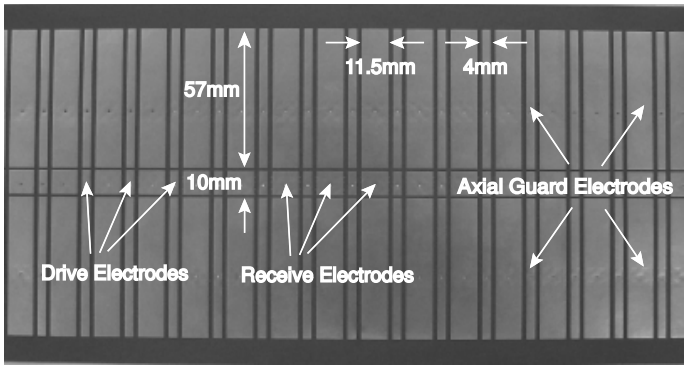

Figure 2. Picture of the single-drive interleaved sensor used in our ECT system.

We demonstrate its performance in numerical simulations and actual experiments.

2. Mathematical Theory and Algorithm

2.1. Model Problem and ECT Setup

Let $z-$axis be the longitudinal direction of the pipeline. We assume that the cross section of the pipe is a disk with radius r_p which will be denoted by Ω. We attach $2N$ electrodes along the pipe in such a way that N drive and N receive electrodes are placed alternately as shown in figure 1(a) and figure 2. The length of all electrodes is 10mm, while widths of the drive and receive electrodes are 4 and 11.5mm, respectively. We also attach axial guards and a grounded screen on the exterior of the sensor to prevent external electrical noise from entering the system. We denote the drive electrodes by $E_1^d, \cdots, E_N^d$ and receive electrodes by $E_1^c, \cdots, E_N^c$. We apply a fixed positive voltage, V to all drive electrodes E_j^d $(j = 1, \cdots, N)$, while grounding all receive electrodes E_j^c $(j = 1, \cdots, N)$. This gives rise to electric field $\mathbf{E}$ and the corresponding electric potential u with $\mathbf{E} = -\nabla u$ satisfying $\nabla \cdot ((\sigma(\mathbf{r}) + i\omega\varepsilon(\mathbf{r}))\nabla u(\mathbf{r})) = 0$ inside the pipe with the boundary conditions; $u = V$ on the drive electrodes $\cup_{j=1}^N E_j^d$ and $u = 0$ on the receive electrodes $\cup_{j=1}^N E_j^c$. Here, ε and σ are the permittivity and conductivity distribution inside the pipe, respectively. In this model, we assume that the pipe wall except for the surface of the electrodes is grounded.

Suppose an object(such as sea water) having higher permittivity and conductivity occupies a region inside the pipe and is surrounded by a background with a much lower permittivity (such as oil). While the relative permittivity of oil is 2.3, the relative permittivity of sea water is 72 and its conductivity is around 4(S/m) Cheng 1989). The goal is to provide a cross-sectional image of the pipe at the plane $z = 0$ from a single measurement of the capacitance $C[j]$ along the electrodes $E_j^c, j = 1, \cdots, N$. The measured capacitance can be expressed as

$$C[j] = \frac{-1}{V} \int_{E_j^c} \varepsilon \, \mathbf{n} \cdot \nabla u \, dA, \quad j = 1, \cdots, N \tag{1}$$

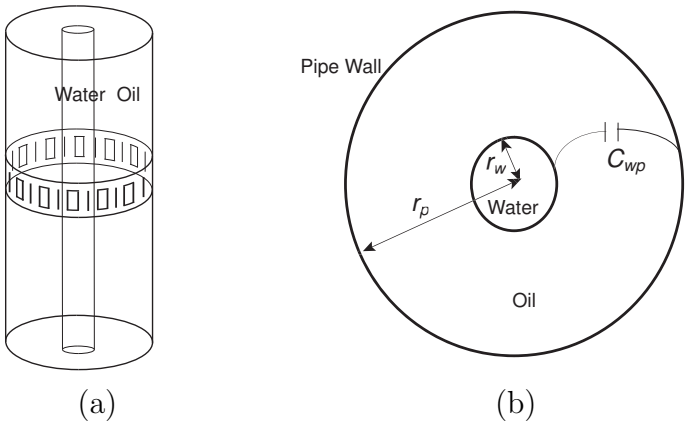

Figure 3. (a) Configuration of a cylindrical water region inside the pipeline and (b) its cross-sectional view.

where $\mathbf{n}$ is the unit outward normal vector to the boundary and dA the surface area element.

In the proposed ECT system, we must consider two dimensional mathematical framework when the size of the water region having relatively higher conductivity is much larger than the size of electrodes. Note that the pipe wall except for the surface of the electrodes is grounded. We assume that the water region is a cylindrical domain centered at the origin with radius r_w and length L_w as shown in figure 3. In this case, the capacitance between the water region and the pipe wall can be calculated (Cheng 1989) as

$$C_{wp} = \frac{2\pi\varepsilon_{oil}L_w}{ln(r_p/r_w)}.$$

With $\varepsilon_{oil} = 2.3$, $L_w = 10$m and $r_p/r_w = 2$, we get $C_{wp} \approx 1.84$nF. At the operating frequency of 1MHz, the impedance between the pipe wall and the water region is approximately 88Ω and, therefore, the water region can be regarded as being effectively connected to the pipe wall at the ground potential. Furthermore, since the conductivity of brine is much higher than that of oil, the electric potential in the water region is almost uniform. Therefore, if the size of the water region is very large compared with the size of electrodes, the electric potential inside the water region is very close to zero, that is,

$$u \approx 0 \quad \text{in the region of water.}$$

Figure 4 is a two-dimensional simulation showing how the potential inside the conductor becomes zero as the length of the conductor becomes longer.

Now, we are ready to set up a two-dimensional mathematical model. Let B_r denote the disk with radius r centered at the origin. For convenience, we assume that drive and receive electrodes are arranged on the unit circle ∂B_1 and the thickness of the pipe wall is δ. Denote $\Omega = B_1$. Let D be the cross-section of a grounded conductor region cut by the plane $z = 0$ and $D \subset B_{1-\delta}$. For simplicity, we assume that the permittivity ε inside $B_1 \setminus \overline{D}$ is constant. If the applied voltage V is 1, the voltage $u(x, y) := u(x, y, 0)$

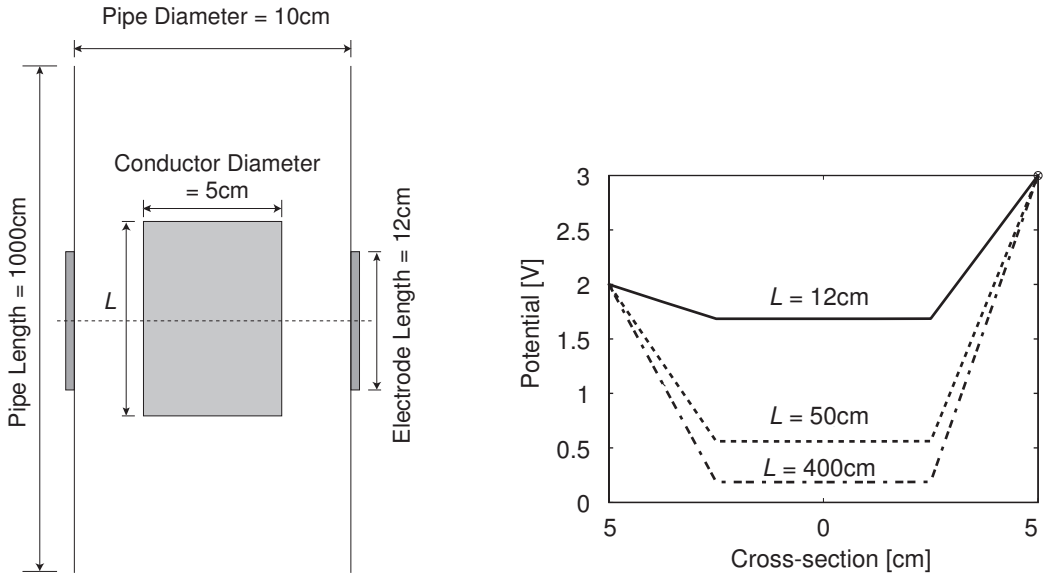

Figure 4. (a) Two-dimensional example of a grounded conductor: a conductor with hight L is placed at the center of a pipe with 10cm diameter and 1000cm length. (b) Potential distribution at the middle cross-section when L =12, 50 and 400cm. As the length of the conductor L becomes longer, the potential inside the conductor approaches zero ground potential.

satisfies

$$\begin{cases} \nabla^2 u(x,y) = 0 \quad \text{in } \Omega \setminus \bar{D} \\ u = 0 \quad \text{in } D \\ u = 1 \quad \text{on each } \tilde{E}_j^d \qquad \text{and} \qquad u = 0 \quad \text{on each } \tilde{E}_j^c \end{cases} \tag{2}$$

where $\tilde{E}_j^c = E_j^c \cap \{z = 0\}$ and $\tilde{E}_j^d = E_j^d \cap \{z = 0\}$. Let u_0 be the corresponding voltage of (2) in the absence of D. We denote

$$g := \mathbf{n} \cdot \nabla u|_{\partial\Omega}, \quad g_0 := \mathbf{n} \cdot \nabla u_0|_{\partial\Omega}, \quad \rho := \mathbf{n} \cdot \nabla u|_{\partial D}.$$

Using the capacitance measurements, we can compute a two-dimensional version of capacitance difference:

$$c_j = \int_{\tilde{E}_j^c} \mathbf{n} \cdot \nabla(u - u_0)\, ds = \int_{\tilde{E}_j^c} (g - g_0)\, ds \tag{3}$$

where ds is the length element. In our ECT system, we do not measure Neumann data on the drive electrodes $E_1^d, \cdots, E_2^d$. Hence, Neumann data is available in a part of the boundary $\partial\Omega$ and the previous layer potential method of finding inhomogeneities is not applicable.

The goal is to develop a real-time algorithm for imaging D from the capacitance data $c_1, \cdots, c_N$. Let us collect properties of the potential u that can be obtained from well known results in partial differential equation such as the standard maximum principle and Hopf's lemma:

- $c_k = 0$ for all $k = 1, \cdots, N$ if and only if $D = \emptyset$.
- If $D \neq \emptyset$, $u < u_0$ in $\Omega \setminus D$.
- $\rho := \mathbf{n} \cdot \nabla u|_{\partial D} > 0$ on ∂D and $\int_{\partial D} \rho ds = \int_{\partial\Omega} g ds$.

2.2. Relation Formula between Water Region and Capacitance Data

Throughout this section, we assume that D is a non-empty open set with smooth boundary. In order to extract some information of the grounded region D, we try to find an explicit and quantitative relation between D and the capacitance data $c_1, \cdots, c_N$ in (3).

In this section, we derive the following approximate identity that plays a key role in tracking the water region D.

Observation 2.1 *We have the following idenity*

$$c_k = \frac{1}{2\pi} \int_{\tilde{E}_k^c} \int_{\partial D} \frac{1 - (x')^2 - (y')^2}{(\cos\theta - x')^2 + (\sin\theta - y')^2} \, \rho(x', y') \, ds d\theta, \quad k = 1, 2, \cdots, N. \tag{4}$$

This can be approximated as

$$c_k \approx \frac{\beta}{2\pi} \int_{\partial D} \frac{1 - x^2 - y^2}{(\cos\theta_k - x)^2 + (\sin\theta_k - y)^2} \, \rho(x, y) \, ds \qquad k = 1, 2, \cdots, N \tag{5}$$

where $(\cos\theta_k, \sin\theta_k)$ *is the center point of the electrodes* $\tilde{E}_k^c$ *and* β *the width of receive electrodes.*

Proof of Observation 2.1. If $\sqrt{x^2 + y^2} > 1$, it follows from Green's theorem that

$$\begin{aligned} 0 &= \tfrac{1}{2\pi} \textstyle\int_\Omega \nabla^2 \log \sqrt{(x' - x)^2 + (y' - y)^2} \, u(x', y') dA \\ &= \tfrac{-1}{2\pi} \textstyle\int_{\partial\Omega} \frac{\mathbf{n} \cdot (x - x', y - y')}{(x - x')^2 + (y - y')^2} \, u(x', y') ds \; - \; \mathcal{S}[g](x, y) \\ &\quad + \tfrac{1}{2\pi} \textstyle\int_{\partial D} \log \sqrt{(x' - x)^2 + (y' - y)^2} \; \rho(x', y') \, ds \end{aligned} \tag{6}$$

where $\mathcal{S}[g](x, y)$ is the single layer potential defined by

$$\mathcal{S}g(x, y) := \frac{1}{2\pi} \int_{\partial\Omega} \log \sqrt{(x' - x)^2 + (y' - y)^2} \, g(x', y') \, ds.$$

Similar identity holds for u_0:

$$0 = \frac{-1}{2\pi} \int_{\partial\Omega} \frac{\mathbf{n} \cdot (x - x', y - y')}{(x - x')^2 + (y - y')^2} \, u_0(x', y') ds - \mathcal{S}g_0(x, y), \quad \text{for} \quad \sqrt{x^2 + y^2} > 1. \tag{7}$$

Since $u = u_0$ on $\partial\Omega$, subtracting (6) from (7) yields

$$\mathcal{S}[g - g_0](x, y) = \frac{1}{2\pi} \int_{\partial D} \log \sqrt{(x' - x)^2 + (y' - y)^2} \; \rho(x', y') \, ds, \text{ for } \sqrt{x^2 + y^2} > 1. \tag{8}$$

In our ECT system, we have c_j, $j = 1, \cdots, N$ and we do not know Neumann data g on the boundary $\partial\Omega \setminus \cup_{j=1}^N \tilde{E}_j^c$. Thus we cannot use the above identity (8) for searching D directly. We must modify the above identity (8) to extract the information of the

target D from the measured data $c_j, j = 1, \cdots, N$. We use the following trace formula in potential theory (Folland 1976):

$$\lim_{t\to 1^+} \langle (x,y)\ ,\ \nabla \mathcal{S}[g](tx,ty)\rangle = \frac{1}{2} g(x,y)\ +\ \mathcal{T}g(x,y), \quad \text{for } (x,y)\in\partial\Omega \tag{9}$$

where

$$\mathcal{T}g(x,y) = \frac{1}{2\pi}\int_{\partial\Omega} \frac{(x,y)\cdot(x-x',y-y')}{(x-x')^2+(y-y')^2}\ g(x',y')\ ds.$$

We apply this trace formula (9) to (8) and obtain

$$\frac{1}{2}[g-g_0](x,y) + \mathcal{T}[g-g_0](x,y)\ =\ \frac{1}{2\pi}\int_{\partial D} \frac{(x,y)\cdot(x-x',y-y')}{(x-x')^2+(y-y')^2}\ \rho(x',y')\ ds \tag{10}$$

for $(x,y)\in\partial\Omega$. The circular geometry of Ω provides the following identity

$$\frac{(x,y)\cdot(x-x',y-y')}{(x-x')^2+(y-y')^2} = \frac{1-xx'-yy'}{2-2xx'-2yy'} = \frac{1}{2}, \quad \text{for } (x,y),(x',y')\in\partial\Omega.$$

We take an advantage of the circular geometry of Ω to derive the following key identity:

$$\mathcal{T}[g-g_0](x,y) = \frac{1}{4\pi}\int_{\partial\Omega}(g-g_0)ds = \frac{1}{4\pi}\int_{\partial\Omega} g ds = \frac{1}{4\pi}\int_{\partial D}\rho\ ds.$$

Here, we use the fact that $\int_{\partial\Omega} g_0 ds = 0$ and

$$0 = \int_{\Omega\setminus D}\nabla^2 u dA = \int_{\partial\Omega} g ds - \int_{\partial D}\rho ds.$$

Hence, the identity (10) becomes

$$[g-g_0](x,y)\ =\ \frac{-1}{2\pi}\int_{\partial D}\rho ds + \frac{1}{\pi}\int_{\partial D}\frac{1-xx'-yy'}{(x-x')^2+(y-y')^2}\ \rho(x',y')\ ds.$$

The above identity can be simplified as

$$[g-g_0](\sin\theta,\cos\theta)\ =\ \frac{1}{2\pi}\int_{\partial D}\frac{1-(x')^2-(y')^2}{(\cos\theta-x')^2+(\sin\theta-y')^2}\ \rho(x',y')\ ds$$

which provides the relation between data c_k and D as follows:

$$c_k\ =\ \frac{1}{2\pi}\int_{\tilde{E}_k^c}\int_{\partial D}\frac{1-(x')^2-(y')^2}{(\cos\theta-x')^2+(\sin\theta-y')^2}\ \rho(x',y')\ ds d\theta, \quad k=1,2,\cdots,N.$$

The formula (5) follows from approximating the integral $\int_{\tilde{E}_k^c}$ by evaluating θ at θ_k and multiplying by the width β of $\tilde{E}_k^c$.

2.3. Location Estimation

In this section, we investigate an accurate location information of D based on the identity (5).

Observation 2.2 *Assume D is connected. For each $k \neq l$ $(k, l = 1, \cdots, N)$, we define a "intersecting" circle $\mathcal{C}_{k,l}$ by*

$$\mathcal{C}_{k,l} := \left\{ (x,y) \in \mathbb{R}^2 \mid \quad c_k \frac{[(\cos\theta_k - x)^2 + (\sin\theta_k - y)^2]}{[(\cos\theta_l - x)^2 + (\sin\theta_l - y)^2]} = c_l \right\}. \tag{11}$$

We have the following observations:

- *Every circle $\mathcal{C}_{k,l}$ intersects the water region $\bar{D}$.*
- *One intersection point between two circles $\mathcal{C}_{k,l}$ and $\mathcal{C}_{k',l'}$ lies in the convex hull of D.*

Let us briefly explain the reasoning behind the first of the above statements. If the above statement is not true,

$$D \quad \subset \quad \mathcal{R}^+_{k,l} \qquad \text{or} \qquad \overline{D} \cap \mathcal{R}^+_{k,l} = \emptyset$$

where

$$\mathcal{R}^+_{k,l} := \left\{ (x,y) \in \mathbb{R}^2 \mid \quad c_k \frac{[(\cos\theta_k - x)^2 + (\sin\theta_k - y)^2]}{[(\cos\theta_l - x)^2 + (\sin\theta_l - y)^2]} \; > \; c_l \right\}.$$

Hence, if $\overline{D} \subset \mathcal{R}^+_{k,l}$, we have

$$\frac{c_k}{[(\cos\theta_l - x)^2 + (\sin\theta_l - y)^2]} \; > \; \frac{c_l}{[(\cos\theta_k - x)^2 + (\sin\theta_k - y)^2]} \quad \text{for all } (x,y) \in D.$$

According to (5), the above inequality leads to the following contradiction:

$$\begin{aligned} c_l c_k &= c_l \, \frac{\beta}{2\pi} \int_{\partial D} \frac{(1 - x^2 - y^2)\, \rho(x,y)}{(\cos\theta_k - x)^2 + (\sin\theta_k - y)^2} \; ds \\ &< \; c_k \, \frac{\beta}{2\pi} \int_{\partial D} \frac{(1 - x^2 - y^2)\, \rho(x,y)}{(\cos\theta_l - x)^2 + (\sin\theta_l - y)^2} \; ds = c_k c_l. \end{aligned}$$

In the case where $\overline{D} \cap \mathcal{R}^+_{k,l} = \emptyset$, we can get a similar contradiction.

Before closing this subsection, we must mention one minor mathematical point. Since the identity (5) is only approximate, the above statement is only approximately true. However, as the width of the receiver electrodes tends to zero, (5) becomes exact and the statement about the location becomes exactly true. We believe that the result can be made precise even for electrodes of finite length, but we have not included the details here in the interests of brevity.

2.4. Rough Shape Estimation

In this section, we try to estimate a rough distance from each electrode $\tilde{E}^c_j$ to the grounded conducting region using c_j. This distance estimation using measured data $c_1, \cdots, c_N$ provides a rough shape of D.

Recall that $D \subset B_{1-\delta}$. For each $0 < r < 1 - \delta$, the potential in (2) with D replaced by B_r will be denoted by u_r. We define a function

$$\eta(r) := \int_{\tilde{E}^c_1} \mathbf{n} \cdot \nabla(u_r - u_0) \; ds \qquad \text{for} \quad 0 \leq r \leq 1 - \delta.$$

From the standard maximum principle in Laplace equation, we have the following properties that will be used in the distance estimation from the electrode $\tilde{E}_k^c$ to D:

$$D \subset B_r \quad \Rightarrow \quad c_k \leq \eta(r) \qquad \text{and} \qquad B_r \subset D \quad \Rightarrow \quad c_k \geq \eta(r). \tag{12}$$

To see the first implication, if $D \subset B_r$, then $u_r \leq u$ in $\Omega \setminus B_r$, so $\mathbf{n} \cdot \nabla(u_r - u_0)|_{\tilde{E}_k^c} \geq \mathbf{n} \cdot \nabla(u - u_0)|_{\tilde{E}_k^c}$ leading to $\eta(r) \geq c_k$. The second implication follows in a similar way.

From the maximum principle, η is strictly increasing in the interval $[0, 1-\delta]$ and $0 = \eta(0) \leq c_k \leq \eta(1-r)$. Hence, we can find a unique r_k such that

$$\eta(r_k) = c_k \qquad \text{for } k = 1, \cdots, N.$$

From this, we roughly approximate the distance between $\tilde{E}_k^c$ and D by r_k.

Observation 2.3 *Let $\gamma(\theta), 0 \leq \theta \leq \pi$ be a smooth curve (for example a spline or trigonometric polynomial of a given degree) such that $\gamma(\theta_k) = r_k,\ k = 1, \cdots, N$. Then we roughly guess D as*

$$\{(x, y) = (r\cos\theta, r\sin\theta) \ : \ \sqrt{x^2 + y^2} = r < \gamma(\theta), \quad 0 \leq \theta \leq 2\pi\}. \tag{13}$$

2.5. Size Estimation

In EIT, novel size estimation methods have been proposed for the inclusion D entering the conductivity equation $\nabla \cdot ((1 + \mu\chi_D)\nabla u) = 0$ with $-1 < \mu \neq 0 < \infty$ (Alessandrini *et al* 2000; Kwon and Seo 2001; Kim *et al* 2002; Kwon *et al* 2002; Kwon *et al* 2003). However, in the case where D is perfectly insulating ($\mu = -1$) or perfectly conducting ($\mu = \infty$), these size estimations should not hold without imposing geometric constraint of D such as convexity.

In our model, it should be noticed that it is impossible to estimate the size of general shape of D from the Cauchy data. Indeed, if D_1 and D_2 have the same outermost boundary, the corresponding voltages have the same Cauchy data on $\partial\Omega$, while it could be $D_1 \neq D_2$ without geometric constraints such as simply connectedness. In this section, we propose a method of estimating a rough size of D when D is convex and the largest diameter of D is comparable to the smallest diameter of D. The proposed size estimation method is not satisfactory since we use a Neumann data g on the drive electrodes that is not available in practice. Hence, the size estimate is not reliable and not accurate due to the use of guessed Neumann data g on the drive electrodes. However, we want to include the following less practical size estimation result in this paper because it gives some information of the size.

Observation 2.4 *Assume $D \neq \emptyset$. Let $\mathbf{r}_0 = (x_0, y_0)$ be an intersection point between two circles $\mathcal{C}_{k,l}$ and $\mathcal{C}_{k',l'}$. (This $\mathbf{r}_0$ can be chosen using the location search method of the previous section.) Define*

$$d_{\mathbf{r}_0} := \exp\left[\frac{2\pi}{\int_{\partial\Omega} g\ ds}\ \int_{\partial\Omega}\left(\frac{1}{2\pi}\log|\mathbf{r}_0 - \mathbf{r}|g(\mathbf{r}) - \frac{\mathbf{n}\cdot(\mathbf{r}-\mathbf{r}_0)}{2\pi|\mathbf{r}-\mathbf{r}_0|}\ f(\mathbf{r})\right)\ ds_{\mathbf{r}}\right] \tag{14}$$

where $\mathbf{r} = (x, y)$. Then there exists $\mathbf{r}^* \in \partial D$ such that $d_{\mathbf{r}_0} = |\mathbf{r}_0 - \mathbf{r}^*|$. We guess that the size of D is $\pi d_{\mathbf{r}_0}^2$.

Please note that $\int_{\partial\Omega} g > 0$ since $D \neq \emptyset$. Let us give the proof of the above observation. For $\mathbf{r}_0 = (x_0, y_0) \in D$, Green identity gives

$$0 = u(\mathbf{r}_0) = \int_{\partial\Omega} \frac{\mathbf{n}\cdot(\mathbf{r}-\mathbf{r}_0)}{2\pi|\mathbf{r}-\mathbf{r}_0|} f(\mathbf{r})ds - \mathcal{S}g(\mathbf{r}_0) + \int_{\partial D} \frac{1}{2\pi}\log|\mathbf{r}_0-\mathbf{r}|\rho(\mathbf{r})\ ds_{\mathbf{r}}. \tag{15}$$

Since $\Phi(\mathbf{r}_0,\mathbf{r}) = \frac{1}{2\pi}\log|\mathbf{r}-\mathbf{r}_0|$ is increasing as $|\mathbf{r}-\mathbf{r}_0|$ increases, there exists $\mathbf{r}^* \in \partial D$ such that

$$\int_{\partial D} \frac{1}{2\pi}\log|\mathbf{r}_0-\mathbf{r}|\ \rho(\mathbf{r})\ ds_{\mathbf{r}} = \frac{1}{2\pi}\log|\mathbf{r}_0-\mathbf{r}^*| \int_{\partial D} \rho(\mathbf{r})\ ds_{\mathbf{r}}.$$

Since $\int_{\partial\Omega} g\ ds = \int_{\partial D} \rho\ ds$, we obtain

$$\int_{\partial D} \frac{1}{2\pi}\log|\mathbf{r}^*-\mathbf{r}_0|\rho(\mathbf{r})\ ds_{\mathbf{r}} = \frac{1}{2\pi}\log|\mathbf{r}^*-\mathbf{r}_0| \int_{\partial\Omega} g(\mathbf{r})\ ds_{\mathbf{r}}.$$

Hence, it follows from (15) that

$$\int_{\partial\Omega} \left[\frac{1}{2\pi}\log|\mathbf{r}-\mathbf{r}_0|g(\mathbf{r}) - \frac{\mathbf{n}\cdot(\mathbf{r}-\mathbf{r}_0)}{2\pi|\mathbf{r}-\mathbf{r}_0|}\ f(\mathbf{r})\right]\ ds_{\mathbf{r}} = \frac{1}{2\pi}\log|\mathbf{r}^*-\mathbf{r}_0| \int_{\partial\Omega} g(\mathbf{r})\ ds_{\mathbf{r}}. \tag{16}$$

3. Numerical Simulation and Experimental Results

We performed both numerical simulations and actual experiments to test the feasibility of the estimation methods described in the previous section. We used sixteen receive electrodes $E_1^c, E_2^c, ..., E_{16}^c$ and sixteen drive electrodes $E_1^d, E_2^d, ..., E_{16}^d$. For different configurations of a grounded conductor D, we applied the estimation methods in the following three steps.

- For the location estimation of D using the formula (11), we perform the following steps.
  - (i) Pick a pair of electrodes E_k^c and E_l^c lying at opposite sides and draw a circle using the formula (11).
  - (ii) Pick a pair of electrodes $E_{k'}^c$ and $E_{l'}^c$ located at 90° orientation from E_k^c and E_l^c and draw another circle.
  - (iii) Pinpoint a intersection point in Ω of the two circles from the previous steps.
  - (iv) Repeat the process for other pairs of electrodes.
  - (v) Plot the point $\mathbf{r}^*$ that is the average of all intersection points obtained from this repeated procedure.
- For the rough shape estimation, we plot a shape of D using the method (13) if $|\mathbf{r}^*| \leq r_0$ where $\mathbf{r}^*$ is the intersection point obtained from the previous location estimation and r_0 is an appropriately chosen number with $0 < r_0 < 1$. If $|\mathbf{r}^*| > r_0$, draw the rough shape of D by applying the adjusted method of (13) with the origin replaced by $\mathbf{r}^*$.
- For the size estimation, we plot a circle with the radius defined in (14).

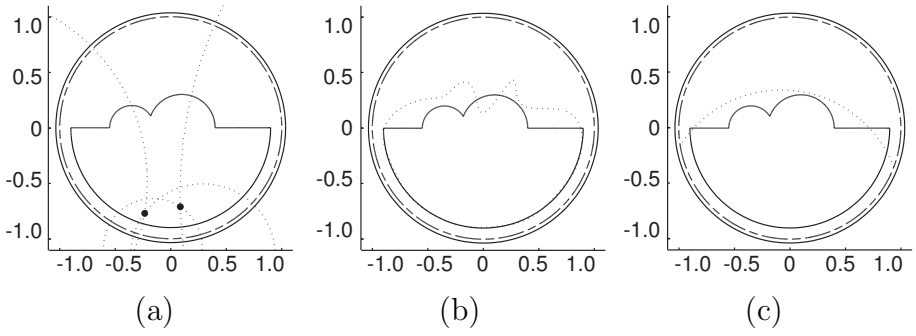

Figure 5. Numerical simulation with a grounded conductor of $\{(x,y)|\ \sqrt{x^2+y^2} < 0.9, y<0\} \cup \{(x,y)|\ \sqrt{(x-0.1)^2+y^2} < 0.3\} \cup \{(x,y)|\ \sqrt{(x+0.35)^2+y^2} < 0.2\}$. (a) Location estimate of $\mathbf{r}^* = (-0.07, -0.74)$. (b) Rough shape estimate. (c) Size estimate with the radius of 0.77.

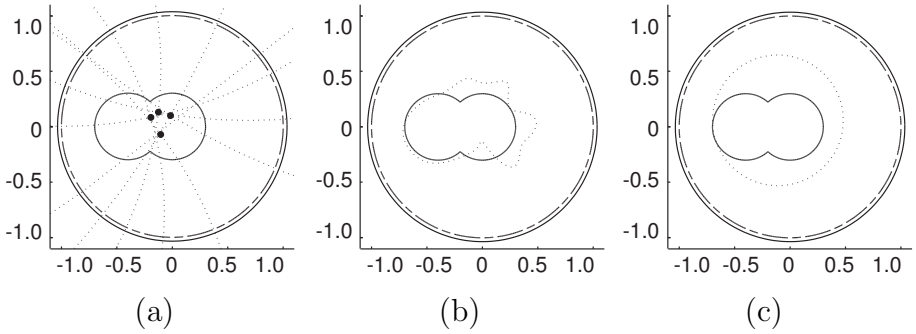

Figure 6. Numerical simulation with a grounded conductor of $\{(x,y)|\ \sqrt{x^2+y^2} < 0.3\} \cup \{(x,y)|\ \sqrt{(x+0.4)^2+y^2} < 0.3\}$. (a) Location estimate of $\mathbf{r}^* = (-0.11, 0.06)$. (b) Rough shape estimate. (c) Size estimate with the radius of 0.42.

3.1. Numerical Simulation Results

Figure 5–9 show the results of numerical simulations with different configurations of the grounded conductor D. In all simulations, we added a random noise of 1.8%. We found that location estimates are reasonably accurate in all cases. The shapes of D located away from the electrodes are relatively poor compared to those near electrodes. This comes from the lower signal-to-noise ratio of the data at receive electrodes located farther away from the grounded conductor. Even though the size estimates could be inaccurate especially for the case of figure 9(c), they still provide useful information on D.

3.2. Experimental Results

For experimental studies, we constructed a single-drive interleaved ECT system. The sixteen drive electrodes are connected to a signal generator. The signal generator is a constant voltage source applying 1MHz sinusoidal voltage signal with 2.25V amplitude to all drive electrodes. We used a 14-bit D/A converter and an FPGA(field programmable gate array) in the signal generator. We measured current on each receive electrode. The

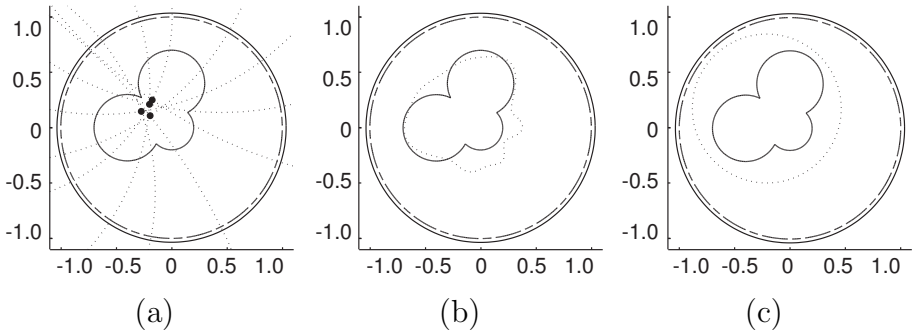

Figure 7. Numerical simulation with a grounded conductor of $\{(x,y)|\ \sqrt{(x+0.4)^2+y^2} < 0.3\} \cup \{(x,y)|\ \sqrt{x^2+(y-0.4)^2} < 0.3\} \cup \{(x,y)|\ \sqrt{x^2+y^2} < 0.2\}$. (a) Location estimate of $\mathbf{r}^* = (-0.21, 0.18)$. (b) Rough shape estimate. (c) Size estimate with the radius of 0.48.

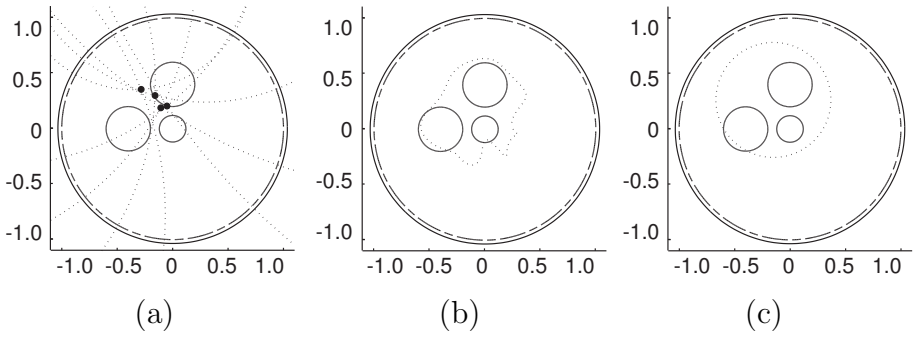

Figure 8. Numerical simulation with a grounded conductor of $\{(x,y)|\ \sqrt{(x+0.4)^2+y^2} < 0.2\} \cup \{(x,y)|\ \sqrt{x^2+(y-0.4)^2} < 0.2\} \cup \{(x,y)|\ \sqrt{x^2+y^2} < 0.12\}$. (a) Location estimate of $\mathbf{r}^* = (-0.15, 0.26)$. (b) Rough shape estimate. (c) Size estimate with the radius of 0.37.

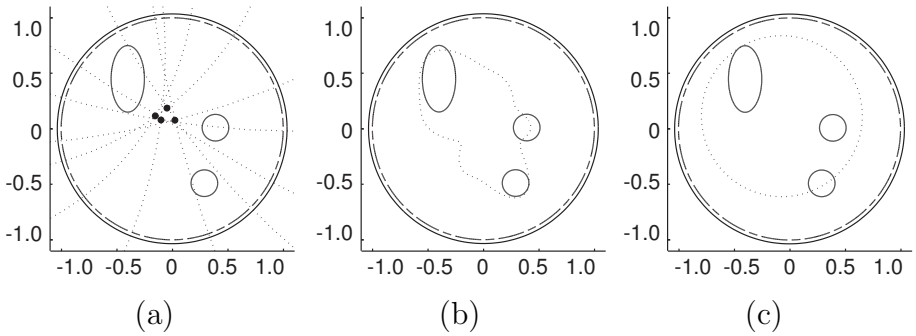

Figure 9. Numerical simulation with a grounded conductor of $\{(x,y)|\ \sqrt{(x-0.39)^2+(y-0.01)^2} < 0.12\} \cup \{(x,y)|\ \sqrt{(x-0.29)^2+(y+0.49)^2} < 0.12\} \cup \{(x,y)|\ \sqrt{4(x+0.4)^2+(y-0.45)^2} < 0.3\}$. (a) Location estimate of $\mathbf{r}^* = (-0.07, 0.11)$. (b) Rough shape estimate. (c) Size estimate with the radius of 0.51.

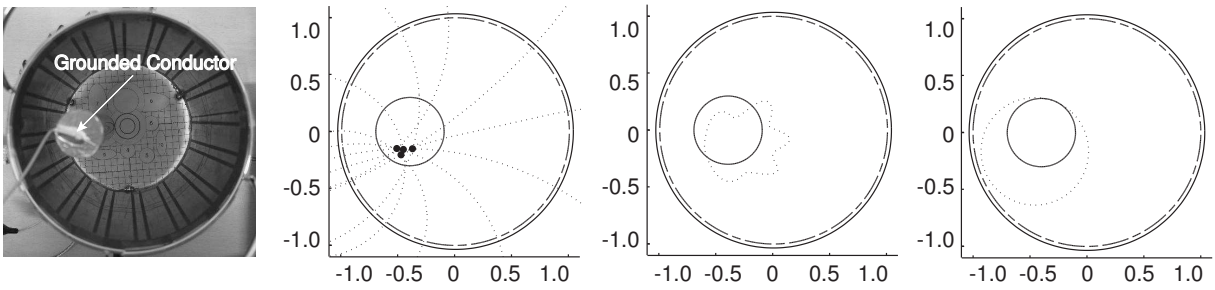

Figure 10. (a) Experimental configuration using a grounded conductor with radius of 0.3 located at (-0.4,0.0).(b) Location estimate of $\mathbf{r}^* = (-0.46, -0.16)$. (c) Rough shape estimate. (d) Size estimate with the radius of 0.33.

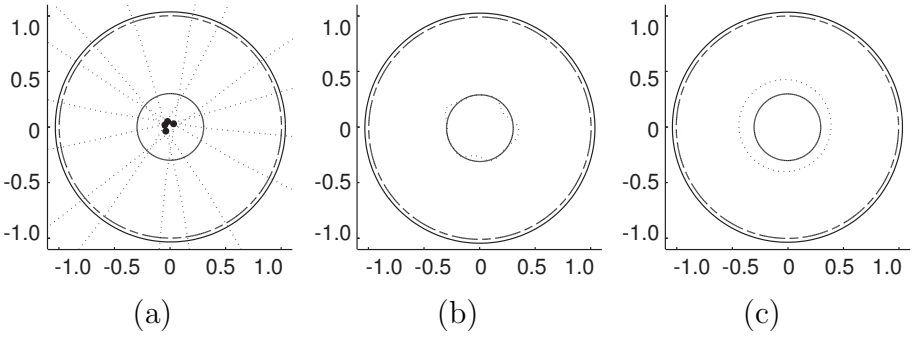

Figure 11. Experimental result using a grounded conductor with radius of 0.3 located at (0,0). (a) Location estimate of $\mathbf{r}^* = (-0.02, 0.01)$. (b) Rough shape estimate. (c) Size estimate with the radius of 0.29.

current measuring circuit consists of a current-to-voltage converter, voltage amplifier, 14-bit A/D converter and FPGA for demodulation. Since we separated the signal generator from the current measuring circuit, we do not need to use any switch to select electrodes between drive and receive modes. Moreover, since equally-spaced sixteen drive electrodes are connected to one signal generator, the standing capacitance is the same for all receive electrodes. So, we do not need to use a programmable gain amplifier to cover a large dynamic range (Yang 1996; Yang and York 1999; Yang 2001). This design can reduce the measurement error and significantly simplifies the required ECT hardware.

Figure 10(a) shows a configuration of a grounded conductor inside the ECT system with 16 drive and 16 receive electrodes. Using the same procedure as in the numerical simulation section, we obtained the results shown in figure 10(b), (c) and (d). In figure 10(b), note that all intersection points are lying inside D. Next, we moved the grounded conductor to the center of the ECT system and repeated the experiment. Figure 10(a), (b) and (c) are the location, rough shape and size estimate, respectively. The experimental results also show the feasibility of the estimation methods.

4. Discussion and Conclusion

Numerical and experimental studies conducted in this paper show promising results for searching a grounded region and estimating its geometric shape and size. From numerous other tests, we found that the location estimation puts all of the intersection points inside the grounded conductor. This is very desirable and suggests the robustness of the location estimate against noise. We found that the accuracy of shape estimate depends on the distance between the edge of the grounded conductor and the nearest electrode. This can be easily understood considering the fact that the sensitivity of a receive electrode decreases as the distance increases.

As illustrated in the size estimation results, the size estimates are not accurate for non-convex domains and it appears that the shape estimation could provide more reliable information for the size of D. However, we speculate that providing all three estimates of location, rough shape and size will be advantageous in practice. Since the algorithms are fast enough for a real-time implementation, one can extract more accurate information on the grounded conductor region by observing dynamical changes of these three estimates.

The main advantage of the proposed ECT system is the use of a single excitation pattern with an interleaved drive and receive sensors to track dynamical changes of a water region in a pipeline. This system significantly simplifies the hardware complexity and reduces measurement noise. In return, we had to limit ourself to a single set of Neumann data available for the estimation of the water region. We could overcome this limitation by developing novel mathematical formulas. These formulas provide concrete relations between a capacitance change in each receive electrode and any dynamical change in the grounded conductor inside the pipeline. The algorithms based on these relations were found to be very useful with the new ECT system. Further experimental works are planned to advance the technique in real industrial applications.

References

Alessandrini G, Rosset E and Seo J K 2000 Optimal size estimates for the inverse conductivity problem with one measurements *Proc. Amer. Math. Soc.* **128** 53-64

Brown B, Barber D, Leathard A, Lu L, Wang W, Smallwood R and Wilson A 1994 High frequency EIT data collection and parametric imaging *Innovation Technol. Biol. Med.* **15** 1-8

Cheng D K 1989 *Field and Wave Electromagnetics* 2nd. ed. (Prentice Hall: NJ, USA)

Folland G B 1976 *Introduction to Partial Differential Equations* (Princeton Univ. Press: NJ, USA)

Kim S, Kwon O and Seo J K 2002 Location search techniques for a grounded conductor *SIAM J. Appl. Math.* **62** 1383-93

Kwon O and Seo J K 2001 Total size estimation and identification of multiple anomalies in the inverse conductivity problem *Inv. Prob.* **17** 59-75

Kwon O, Seo J K and Yoon J R 2002 A real-time algorithm for the location search of discontinuous conductivities with one measurement *Comm. Pure Appl. Math.* **LV** 1-29

Kwon O, Yoon J R, Seo J K, Woo E J and Cho Y G 2003 Estimation of anomaly location and size using electrical impedance tomography *IEEE Trans. Biomed. Eng.* **50** 89-96

Yang W 1996 Hardware design of electrical capacitance tomography systems *Meas. Sci. Technol.* **7** 225-32

Yang W and York T 1999 New AC-based capacitance tomography system *IEE Proc. Sci. Meas. Technol.* **146** 47-53

Yang W 2001 Further developments in an ac-based capacitance tomography system *Rev. Sci. Inst.* **72** 3902-7

Zhu Q S, McLeod C N, Denyer C W, Lidgey F J and Lionheart W R B 1994 Development of a real-time adative current tomograph *Physiol. Meas.* **15** A37-A43